Surgical Endoscopy (2024) 38:3126–3137
https://doi.org/10.1007/s00464-024-10795-x

Assessing the influence of parameters on tissue welding in small bowel end-to-end anastomosis in vitro and in vivo

Caihui Zhu[1] · Yuyan Na[2] · Xiujun Cheng[3] · Xiaonan Tao[1] · Pengyao Xie[1] · Lei Chen[1] · Hui Zhao[1] · Jian Qiu[1] · Xiaodong Gu[4] · Jianbin Xiang[4] · Kefu Liu[1]

Received: 21 December 2023 / Accepted: 9 March 2024 / Published online: 15 April 2024

Abstract

Background The use of high-frequency electric welding technology for intestinal end-to-end anastomosis holds significant promise. Past studies have focused on in vitro, and the safety and efficacy of this technology is uncertain, severely limiting the clinical application of this technology. This study investigates the impact of compression pressure, energy dosage, and duration on anastomotic quality using a homemade anastomosis device in both in vitro and in vivo settings.

Methods Two hundred eighty intestines and 5 experimental pigs were used for in vitro and in vivo experiments, respectively. The in vitro experiments were conducted to study the effects of initial pressure (50–400 kpa), voltage (40–60 V), and time (10–20 s) on burst pressure, breaking strength, thermal damage, and histopathological microstructure of the anastomosis. Optimal parameters were then inlaid into a homemade anastomosis and used for in vivo experiments to study the postoperative porcine survival rate and the pathological structure of the tissues at the anastomosis and the characteristics of the collagen fibers.

Results The anastomotic strength was highest when the compression pressure was 250 kPa, the voltage was 60 V, and the time was 15 s. The degree of thermal damage to the surrounding tissues was the lowest. The experimental pigs had no adverse reactions after the operation, and the survival rate was 100%. 30 days after the operation, the surgical site healed well, and the tissues at the anastomosis changed from immediate adhesions to permanent connections.

Conclusion High-frequency electric welding technology has a certain degree of safety and effectiveness. It has the potential to replace the stapler anastomosis in future and become the next generation of new anastomosis device.

✉ Kefu Liu
kfliu@fudan.edu.cn

[1] School of Information Science and Technology, Fudan University, Shanghai, China

[2] Department of Sports Medicine, Huashan Hospital, Fudan University, Shanghai, China

[3] Department of Dermatology, Huashan Hospital, Fudan University, Shanghai, China

[4] Department of General Surgery, Huashan Hospital, Fudan University, Shanghai, China

Graphical abstract

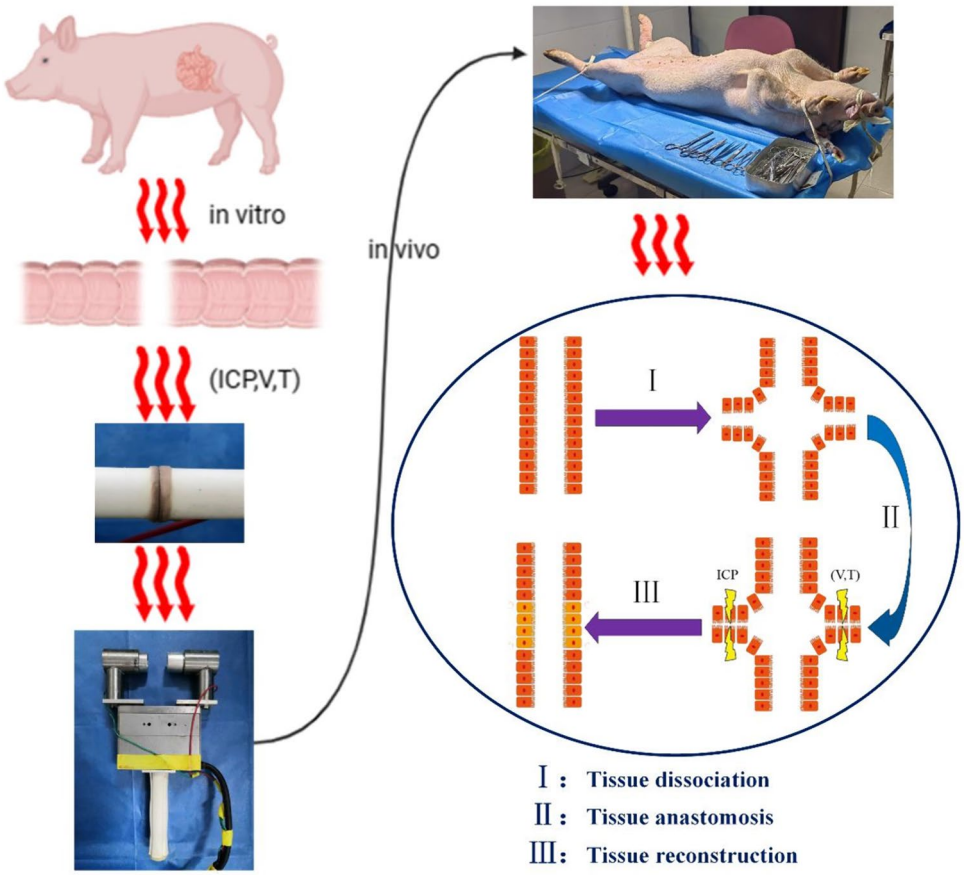

Keywords Intestinal anastomosis · End to end · Electric welding · In vitro · In vivo

Gastrointestinal tract reconstruction is a common surgical procedure, with two main anastomosis techniques: suture and stapler anastomosis. Both methods have high popularity and safety levels; however, each has some drawbacks. Suturing is time-consuming, causes extensive bleeding, and requires high surgical expertise, making it less suitable for laparoscopic operations [1]. Stapler anastomosis, on the other hand, leaves foreign materials in the body, leading to serious secondary injuries [2, 3]. With advancements in modern surgery, particularly the growing preference for minimally invasive techniques, traditional anastomosis methods are increasingly challenged, sparking interest in alternative approaches. High-frequency electric welding (HFEW) can address these issues.

HFEW utilizes autologous soft tissue fusion without foreign material residue, resulting in less bleeding, shorter operation times, and showing great potential for application [4–7]. Developed in the 1990s, HFEW technology, exemplified by the LigaSure system, has been widely used for vascular closure, especially in vessels smaller than 7 mm in diameter, offering more convenience and speed than traditional methods [8–12]. Consequently, surgeons are keen to apply HFEW technology in broader scenarios, such as side-to-side and end-to-end intestinal anastomoses [13, 14].

The success of HFEW technology relies on the tissue's inherent components like Type I collagen and elastin [15, 16]. Joule heating occurs when electric current passes through the tissue, loosening the triple helix structure of Type I collagen monomers and transforming them into randomly coiled peptide chains. Compression of two tissues causes these chains to solidify into a fused mass, creating an immediate adhesive bond [17, 18]. The fusion strength depends not only on the collagen content and tissue thickness but also on compression pressure, energy dosage, and duration [4, 19, 20]. The special healing environment faced by intestinal tissues after anastomosis, end-to-end intestinal anastomosis requires more precise energy application to ensure adequate fusion strength while minimizing thermal damage to surrounding tissues and retaining sufficient viable cells for wound healing. The risk

is heightened due to the intestine's internal contents and susceptibility to infection. In 2010, Winter et al. explored the effect of compression pressure on end-to-end anastomosis in vitro [21]. In 2015, Zhao et al. investigated the effect of electrode shapes on end-to-end anastomosis and thermal injury during tissue fusion [22, 23]. In 2022, Yin et al. explored impedance changes during intestinal fusion in vitro [24]. Despite a decade of attempts by surgeons to use HFEW for gastrointestinal anastomosis, research remains limited to in vitro experiments.

To assess the impact of compression pressure, energy dosage, and duration on anastomotic quality for end-to-end intestinal anastomosis, we employed a homemade pulse generator and an anastomosis device for both in vitro and in vivo experiments. Aim of the in vitro experiments was to assess the effect of initial compression pressure, voltage and time on fusion quality. The in vivo experiments aimed to evaluate the safety and efficacy of HFEW in a porcine model, exploring whether immediate adhesions in the intestine treated with HFEW could be converted into permanent connections during subsequent recovery.

Materials and methods

Ethical approval

Both in vitro and ex vivo experiments were performed under the supervision of a specialized surgeon. All procedures received approval from the Ethics Committee at Shanghai Jiao Tong University (Permit Number 20200701).

Experimental equipment

The anastomotic devices and pulse generator used in this study were developed in-house. The anastomotic device consisted of both ex vivo and in vivo anastomotic equipment. The ex vivo anastomotic device comprised a press machine and copper electrodes with an inner diameter of 13.31 mm and an outer diameter of 23.09 mm (Fig.S1). The in vivo anastomotic device consisted of a small press machine and detachable electrodes, with the same dimensions as the ex vivo equipment (Fig. S2). The pulse generator provided square wave pulses to the intestinal tissue, operating at a frequency of 440 kHz with a duty cycle of 75% (Fig. S3).

In vitro experiments

Fresh small intestine samples were obtained from abattoirs. After thoroughly cleaning the sample contents, they were cut into 10 cm long segments (Fig. 1A) and immersed in a physiological saline solution, stored at 4 °C for later use. In vitro experiments were conducted to optimize three welding parameters, including compression pressure (50 kPa, 100 kPa, 150 kPa, 200 kPa, 250 kPa, 300 kPa, 350 kPa, 400 kPa), voltage (40 V, 50 V, 60 V), and time (10 s, 15 s, 20 s). Tissue fusion was performed using mucosa-to-mucosa end-to-end welding (Fig. 1B), with real-time monitoring of tissue temperature at the anastomotic site using an infrared thermal imager (Fortric-200, Shanghai).

Anastomotic strength testing

Burst pressure testing and breaking strength testing were conducted to assess the quality of the ex vivo intestinal anastomosis [25] (Figs. S4 and S5). Burst pressure represents the maximum pressure at which the anastomotic site ruptures, while breaking strength provides the maximum force at which the anastomotic site tears. Burst pressure below 15.4 mmHg is considered as fusion failure [7].

Pathological evaluation

Tissue from the anastomosis site was cut out after fusion and soaked in formalin solution for HE section staining. Anastomotic site was then sectioned vertically, and histological assessment was performed by an experienced pathologist. In this study, the assessment of thermal injury was performed using pathological assessment [26].

In vivo experiments

24 h before the operation, the experimental pigs ($n = 5$) were fasted and treated, and mannitol was used to clear the intestine. The surgery was operated by a professional surgeon, a 5 cm-long incision was made in the abdomen of the experimental pigs, both ends of the small intestine were clamped with intestinal forceps, part of the mesentery was cut, and then a 15 cm-long intestinal tissue was truncated in the middle, and then the intestinal end-to-end anastomosis was carried out with a homemade anastomosis, and the intestinal mesentery and the abdominal cavity were sutured at the end (Fig. 1C–F). Output voltage waveform of the pulse generator was a square wave with a frequency of 440 kHz, a voltage of 60 V, a time of 15 s and an anastomotic compression pressure of 250kpa.The experimental pigs were fasted for three days after the operation, and were injected with antibiotics daily for 5 days after the operation. Anesthesia, disinfection, postoperative care, and sample collection methods followed established protocols as outlined in published literature [3]. The pigs were monitored continuously for 30 days, observing vital signs, diet, and bowel movements. After this period, they were euthanized, and intestinal tissues

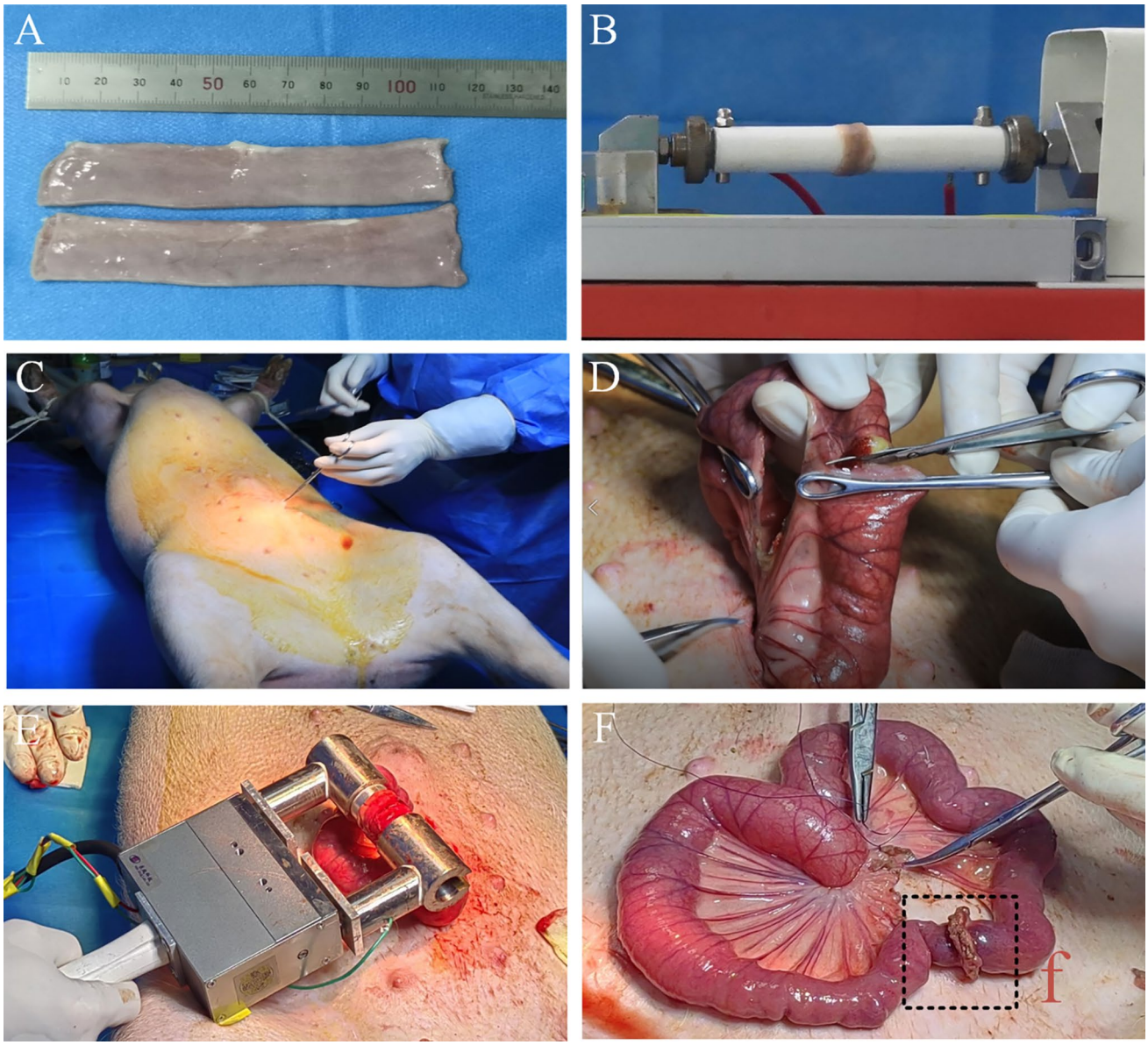

Fig. 1 In vitro and in vivo experiment protocols. **A** Small segments of intestine used for in vitro anastomosis experiments. **B** In vitro small intestine end-to-end anastomosis. **C** Opening laparotomy. **D** Locating the small intestine and transect approximately 15 cm of tissue from the middle. **E** End-to-end anastomosis of the small intestine using a custom-made anastomosis device. **F** Suturing the mesentery after completion of the small intestine anastomosis. The black box is the tissue fusion area. f fusion area

at the anastomosis site were extracted. These tissues were then histologically examined using HE and Masson staining techniques.

Statistical analysis

Data analysis was performed using Prism 8, presenting results as mean ± standard deviation. Intra-group variances were evaluated through ANOVA. All statistical analyses were two-tailed, with significance set at $p < 0.05$. Corresponding figures depict statistical test results (ns, not significant; $*p < 0.05$, $**p < 0.01$, $***p < 0.001$, $****p < 0.0001$) as appropriate.

Results

Effect of compression pressure on anastomotic strength

A total of 160 intestinal samples were used for the optimization experiments on compression pressure, with 80 samples used for burst pressure testing and 80 samples used for tensile strength testing. When the voltage was set at 60 V and the time at 15 s, the burst pressure showed an increasing trend followed by a decrease as the compression pressure increased (Fig. 1A). The welding success rate was 100% when the compression pressure ranged from 150 to 300 kPa, but decreased when the compression pressure exceeded 300 kPa or was below 150 kPa (Table S1).

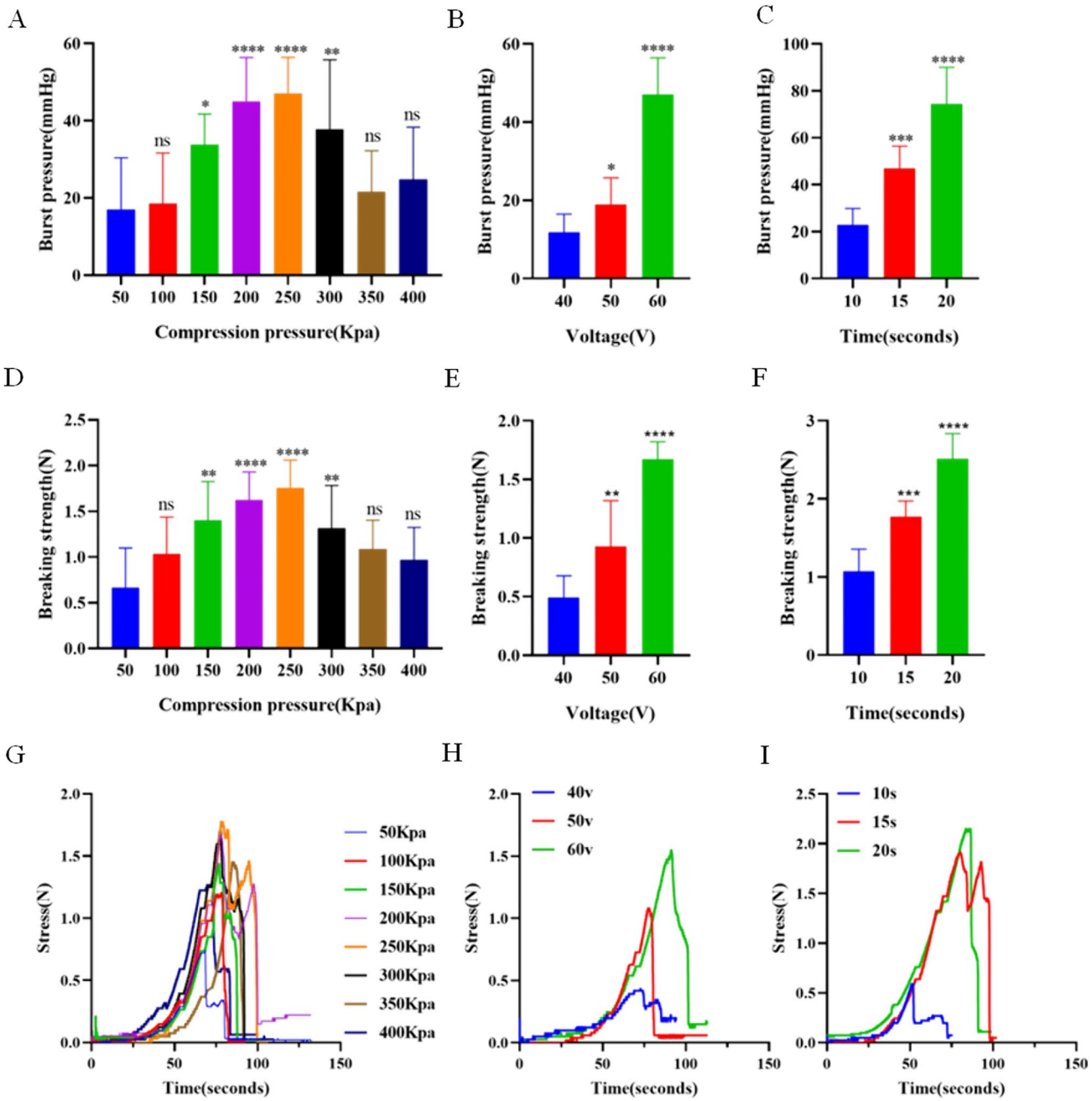

Fig. 2 Intestinal anastomotic strength testing. **A–C** The influence of compressive pressure, voltage, and time on burst pressure, respectively. **D–F** The impact of compressive pressure, voltage, and time on breaking strength, respectively. **G–I** The temporal characteristics of the forces sustained by the intestine over time under different compressive pressures, voltage, and time conditions

Significant differences in burst pressure were observed compared to 50 kPa, with 150 kPa ($p=0.0481$), 200 kPa ($p<0.001$), 250 kPa ($p<0.001$), and 300 kPa ($p=0.0089$) showing significant variations. The highest average burst pressure was observed at 250 kPa (47.07 ± 9.355 mmHg), which was higher than the burst pressure at 200 kPa (45.02 ± 11.3 mmHg) and 300 kPa (37.79 ± 18.1 mmHg).

As the compression pressure increased, the tensile strength initially increased and then decreased (Fig. 2D). Higher median tensile strengths were observed at 150 kPa (1.440N), 200 kPa (1.640N), 250 kPa (1.785N), and 300 kPa (1.395N) (Table S2). Significant differences in tensile strength were found compared to 50 kPa, with 150 kPa ($p=0.0012$), 200 kPa ($p<0.001$), 250 kPa ($p<0.001$), and 300 kPa ($p=0.0063$) showing significant variations (Fig. 1D, G).

Effect of voltage on anastomotic strength

A total of 60 intestinal samples were used for voltage optimization experiments, with 30 for burst pressure tests and 30 for breaking strength tests. As the voltage increased with a compression pressure of 250 kPa and a discharge time of 15 s, the burst pressure rose (Fig. 2B). Success rates were 20% at 40 V, 70% at 50 V, and 100% at 60 V (Table S3). At 60 V, the average burst pressure was highest (47.07 ± 9.355 mmHg), surpassing that of 50 V (18.92 ± 6.875 mmHg) and 40 V (11.79 ± 4.690 mmHg) (Table S3). Tensile strength gradually increased with voltage escalation (Fig. 2E, H) (Table S4), showing significant differences at 50 V ($p=0.0385$) and 60 V ($p<0.001$) compared to 40 V (Table S4).

Effect of time on anastomotic strength

A total of 60 intestinal samples were used for time optimization experiments, with 30 for burst pressure tests and 30 for tensile strength tests. With a compression pressure of 250 kPa and a voltage of 60 V, the burst pressure increased with prolonged discharge time (Fig. 2C). At 10 s, 15 s, and 20 s, success rates were 80%, 100%, and 100%, respectively. At 20 s, the average burst pressure was highest (74.48 ± 15.57 mmHg), surpassing that of 15 s (47.07 ± 9.355 mmHg) and 10 s (22.81 ± 7.078 mmHg) (Table S4). Tensile strength gradually increased with

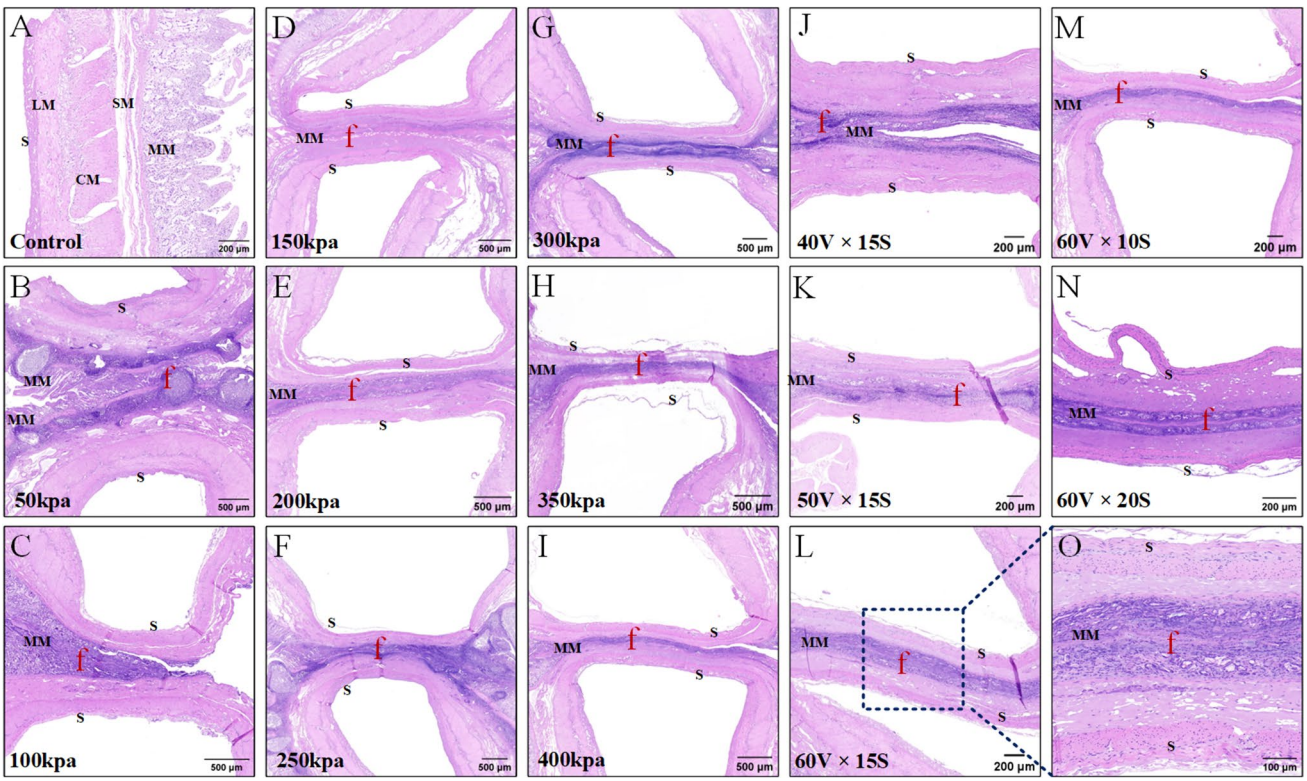

Fig. 3 H&E staining of small intestines. **A** Normal intestinal histopathological structure. **B–I** Characteristics of anastomotic pathological structure with compression pressure when the voltage was 60 V and time was 15S. **J–L** Characteristics of anastomotic pathological structure with voltage. **M–N** Characteristics of anastomotic pathological structure with time. **O** Magnified image of the structure of anastomotic portion when the initial compression pressure was 250 kpa, the voltage was 60 V, and the time was 15S. f fusion area, S serosa, LM longitudinal muscle, CM circular muscle, SM submucosa, MM muscularis mucosa

prolonged time (Fig. 2F, I), showing significant differences at 15 s ($p < 0.001$) and 20 s ($p < 0.001$) compared to 10 s (Fig. 2I).

Pathological structure of the anastomosis

Normal small intestine tissue consists of serosal layer, longitudinal smooth muscle, circular smooth muscle, submucosal layer, and mucosal layer, with a clear and distinct structure (Fig. 3A). In the fusion zone, where the mucosa of the two tissues contacts, the serosa faces outward, and the thickness becomes thinner, with the tissue at the anastomotic site protruding outward. At 50 kPa and 100 kPa, the anastomotic structure is loose, exhibiting larger gaps and spaces (Fig. 3B, C). In the range of 150 kPa to 300 kPa, the tissue structure at the anastomotic site becomes blurred, mucosal tissue is indistinguishable, the overall structure tends to stabilize, and there are no gaps at the anastomotic site (Fig. 3D–G). At 350–400 kPa, the anastomotic structure becomes loose again, gaps reappear, and the quality of the anastomosis decreases (Fig. 3H, I).

Voltage and discharge time impact the pathological structure of the surgical site. As voltage increases, anastomotic gaps gradually disappear, and the quality of anastomosis improves from low to high (Fig. 3J, K), especially at 60 V, where the mucosal area at the anastomotic site merges seamlessly (Fig. 3L). Similarly, with prolonged discharge time, the quality of anastomosis gradually improves. However, at 20 s, the prolonged high temperature leads to increased tissue and electrode adhesion, affecting some serosal structures (Fig. 3L, O).

Temperature changes at the anastomosis

HFEW technology involves tissue fusion induced by collagen thermal denaturation, with a specific temperature being a necessary condition for tissue anastomosis [27]. When the temperature exceeds 60 °C, tissue begins to denature, and as the temperature increases, the interweaving and adhesion of collagen intensify [28, 29]. In Fig. 4A, D, it is shown that the highest temperature at the anastomotic site is related to voltage and time. Figure 4B indicates that at voltages of 40 V, 50 V, and 60 V, the highest temperatures at the anastomotic site are 60.78 ± 1.900 °C, 79.78 ± 2.451 °C, and 89.25 ± 4.375 °C, respectively, with statistically significant differences between different voltages ($p < 0.05$). For times of 10 s, 15 s, and 20 s, the highest temperatures at the anastomotic site are 72.88 ± 6.853 °C, 89.25 ± 4.375 °C, and 90.05 ± 5.544 °C, respectively. Figure 4E shows a significant difference in the highest temperatures between 10 and 15 s ($p < 0.05$), while the difference between 15 and 20 s is not significant ($p > 0.05$). This implies that, after reaching the maximum temperature, extending the time does not increase the temperature, and voltage is the primary parameter determining the anastomotic site temperature.

Tissue thermal damage

As the temperature of the tissue at the anastomosis rises, the temperature of the normal tissue surrounding the anastomosis rises due to heat transfer, resulting in thermal injury. The features of lateral thermal spread include smudging of cell nuclei, feathery appearance of the mucosa (Fig. 4H, I), compaction of the muscularis externa [26].

Figure 4C shows that at voltages of 40 V, 50 V, and 60 V, the thermal injury distances are 0.6133 ± 0.2250 mm, 1.460 ± 0.2910 mm, and 2.487 ± 0.3707 mm, respectively. Figure 4F indicates that at discharge times of 10 s, 15 s, and 20 s, the thermal injury distances are 1.227 ± 0.3528 mm, 2.487 ± 0.3707 mm, and 4.253 ± 0.4461 mm ($p < 0.05$). Different voltages and times exhibit significant differences in thermal injury distances in surrounding tissues, indicating that higher voltages and longer times result in increased thermal injury. In conclusion, based on anastomotic strength and thermal injury distance, it is recommended to use 250 kPa, 60 V, and 15 s for in vivo experiments.

Clinical outcomes

A total of 5 experimental pigs were used for HFEW experiments, and during the surgical procedure, the highest temperature at the anastomotic site reached 92.9 °C (Fig. S6). The average highest temperature at the anastomotic site was 82.5 °C, within the range of collagen denaturation [30]. Postoperative observation revealed that on the third day, experimental pigs resumed intake of feed with a small amount of feces discharged. By the seventh day, they fully resumed both eating and normal bowel movements, indicating that within 7 day post-operation, the levels of food intake and feces elimination returned to pre-surgery levels, signifying basic restoration of intestinal function. There were no significant changes in fecal shape and color, implying the absence of anastomotic fistula or stricture during the recovery period. Throughout the observation period, the survival rate of the domestic pigs was 100%.

Before wound healing, the anastomotic site is relatively fragile, with tissue connections being temporary adhesions (Fig. 5A–C). At 30 days postoperatively, the anastomotic site has undergone remodeling, as depicted in Fig. 5D–F. Observations reveal an infection-free abdominal cavity, smooth surfaces inside and outside the anastomotic site, absence of foreign bodies, no signs of infection or suppuration, no anastomotic fistula, and no occurrence of obstruction. The color and thickness of the surgical site are consistent with the non-operated area. Compared to the tissue immediately after anastomosis, the outwardly protruding necrotic tissue

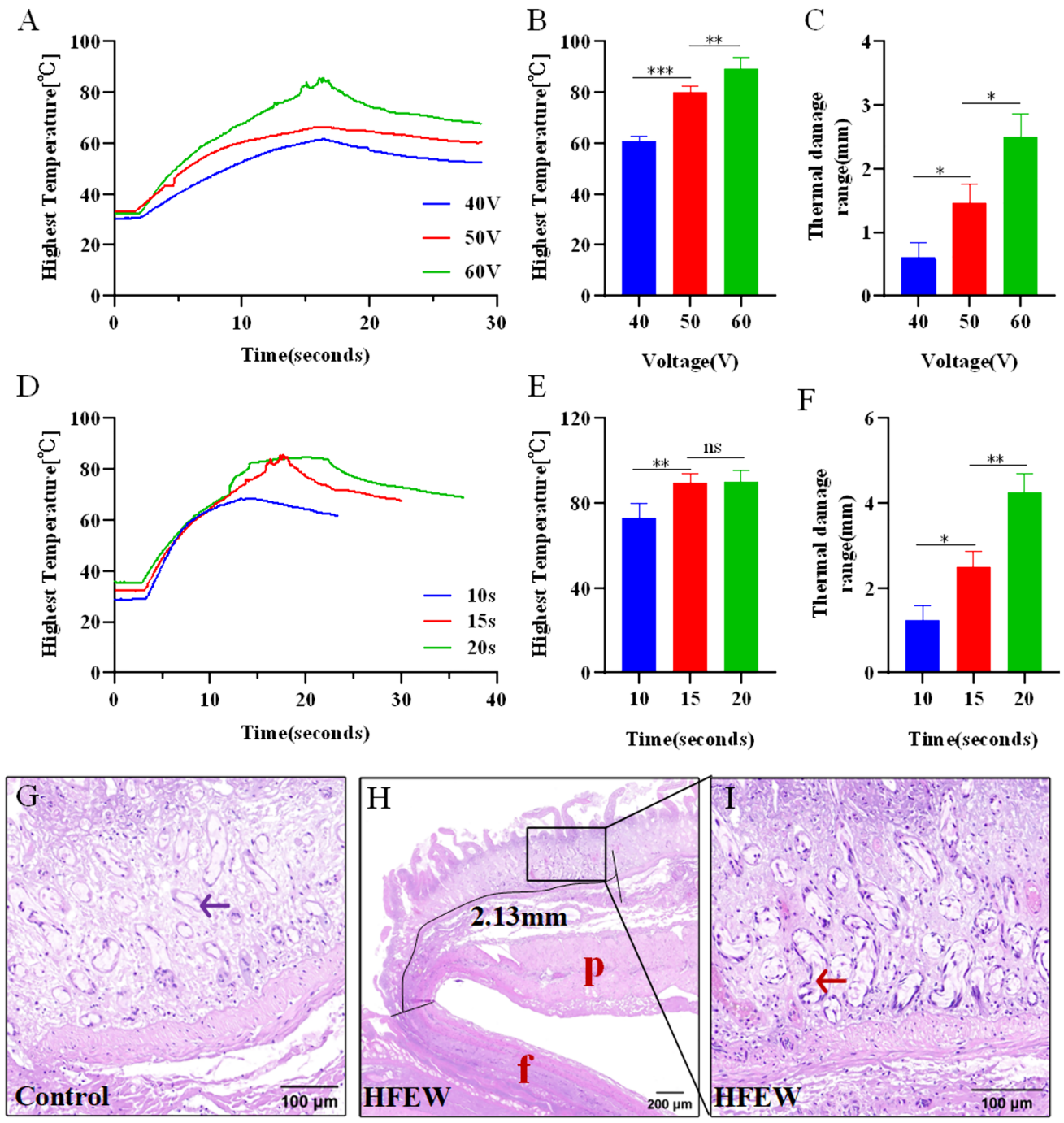

Fig. 4 Characteristic of maximum temperature and thermal damage changes by changing voltage and discharge time. **A**, **D** Characteristics of maximum temperature of tissues at the anastomosis with time. **B**, **E** Maximum temperature of tissues at the anastomosis. **C**, **F** Thermal damage range of peripheral tissues. **G** Normal appearance of mucosa. **H–I**, Feathery appearance of mucosal crypts secondary to thermal damage. f fusion area, p peripheral tissue, blue arrow is normal mucosal tissue, red arrow is thermally damaged mucosal tissue

at the anastomotic site has disappeared (Fig. 5B, E). This suggests the absorption of necrotic tissue by the surrounding tissue. Moreover, the immediate adhesions have transformed into permanent connections (Fig. 5C, F) during the reconstruction of the surgical site.

Architecture of the anastomoses

Compared to normal tissue, the anastomotic site and surrounding tissues form a tight connection, creating a complete closure. Under an optical microscope, the pathological structure of the surgical site is clear, with the formation

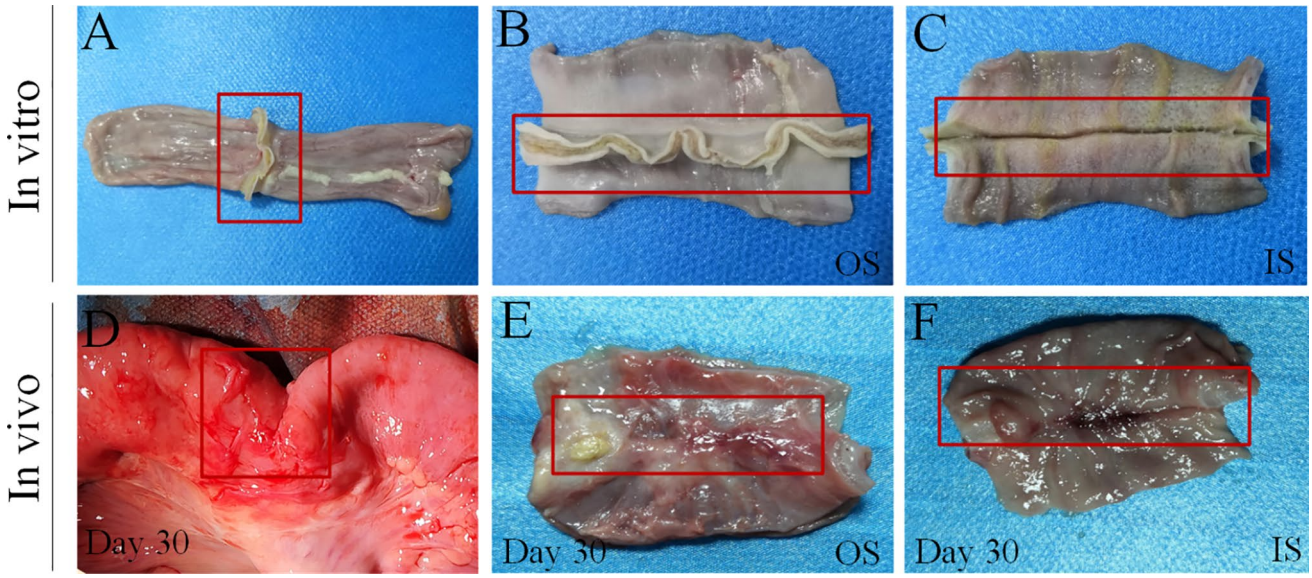

Fig. 5 Structural characteristics of the anastomosis. **A** In vitro experimental anastomosed small bowel. **B**, **C** Outer surface of the anastomosis and internal surface of the anastomosis. **D** Tissue at the anastomosis at 30 days postoperatively. **E**, **F** Outer and Inner surfaces of surgical site. OS outer surfaces, IS Inner surfaces. Anastomotic area in red box

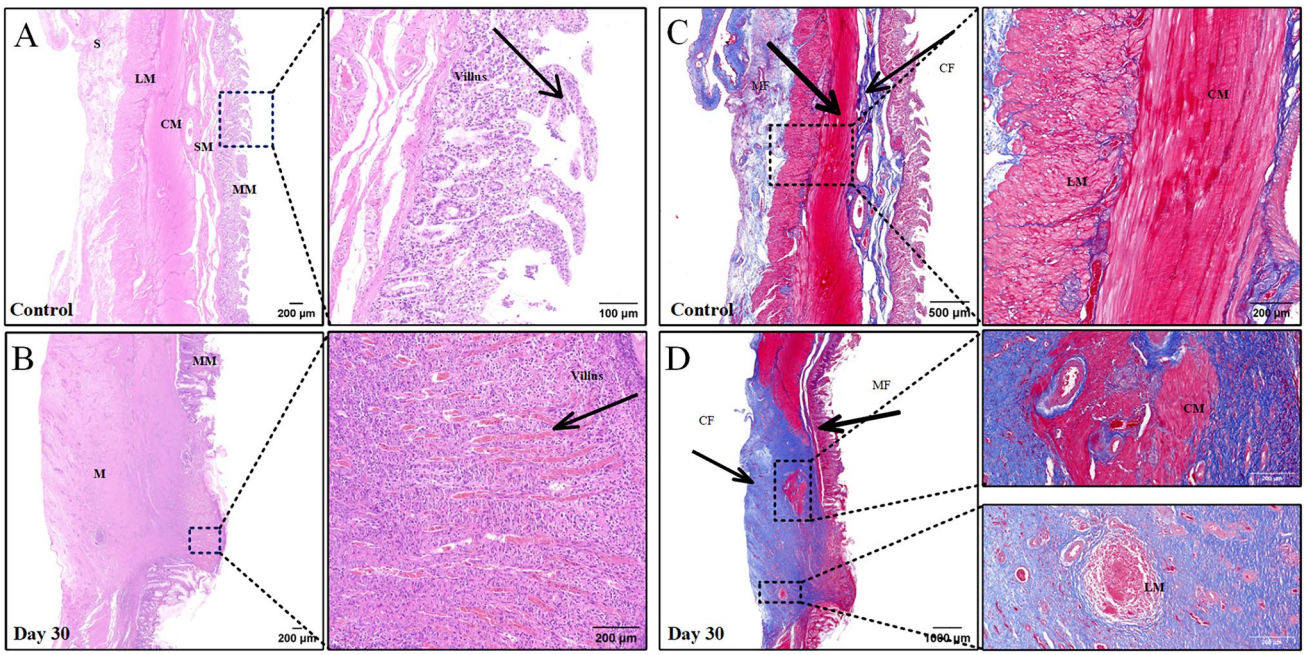

Fig. 6 Characteristics of postoperative recovery in animal models. **A**, **B** Pathological structure and villous structure of normal and surgical site tissues. **C**, **D** Masson staining results of normal and surgical site tissues. The red areas are muscle fibers and the blue areas are collagen fibers. CF collagen fiber, MF myofibers

of a complete mucosal layer and serosal layer. Villi are important structures for the absorption of nutrients by intestinal tissues and are evenly distributed in the intestine [31] (Fig. 6A). Figure 6B shows chorionic granulation at the surgical site, which means that the tissue at the surgical site is about to regain its nutrient-absorbing functions.

In normal tissue, collagen fibers and muscle fibers are uniformly distributed (Fig. 6C), with collagen fibers primarily present in the submucosal layer. As shown in

Fig. 6D, the entire tissue at the anastomotic site contains abundant collagen fibers, with a content higher than that of normal tissue ($p < 0.05$) (Fig. S7). The transverse and longitudinal muscles are crucial structures within the intestinal tract, typically situated between the mucosal and serosal layers in normal tissue. Figure 6D reveals the presence of small clusters of newly formed transverse and longitudinal muscle buds within the collagen fibers at the anastomotic site, with this neo-tissue showing an expanding growth trend. The appearance of newly formed villous buds and regenerated transverse and longitudinal muscle tissue at the anastomotic site indicates an increasingly improved structure and function of the intestinal tissue.

Discussion

The bipolar system used for vascular occlusion cannot directly be applied to intestinal end-to-end anastomosis due to differences in required energy and biological impedance characteristics. Therefore, a completely new anastomosis system tailored for intestinal end-to-end anastomosis is necessary. This system must consider three physical quantities: compression pressure, voltage, and time. This study systematically investigates the impact of these three physical quantities on the quality of anastomosis using an in vitro experimental system and validates these parameters through in vivo experiments.

Compression pressure is a prerequisite for successful tissue welding, essential for both side-to-side and end-to-end intestinal anastomoses. This pressure does not induce collagen denaturation but affects the thickness of the anastomotic site, influencing collagen density and impedance, thus impacting the quality of the anastomosis [23, 32]. Generally, anastomotic strength follows a normal distribution with initial compression pressure. Up to the optimal pressure, anastomotic quality increases with higher initial pressure. Beyond the optimal pressure, anastomotic quality decreases as the initial pressure increases. The optimal range for initial compression pressure in this study is between 150 and 300 kPa. Within this range, there is better anastomotic quality. At 250 kPa, the burst pressure and tensile strength are maximized at 47.07 ± 9.355 mmHg and 1.758 ± 0.3028 N, respectively. At this point, tissue structure at the anastomotic site is challenging to distinguish, with fewer holes and gaps. Beyond this range, anastomotic quality decreases, accompanied by an increase in tissue fusion failure rates.

During the experiments on side-to-side intestinal anastomosis, Arya et al. arrived at the same conclusion that the maximum anastomotic strength was observed at 250 kPa, with a burst pressure of 25.77 ± 4.09 mmHg, beyond which there was a decline in anastomotic quality [25]. Zhao et al. employed convex–concave-shaped electrodes for end-to-end intestinal anastomosis, observing a decrease in burst pressure when the pressure exceeded 277 kPa [22]. In cases of compression pressures below the optimal range, elevated temperatures induced instability between the electrodes, resulting in significant reactive forces pushing the electrodes in the opposite direction, thereby impeding the progression of tissue fusion. As the compression pressure increases, there's a corresponding elevation in biological tissue impedance [33]. Consequently, under similar electrical parameters, the generated heat decreases, which is unfavorable for collagen denaturation. Excessive compression pressure can even result in mechanical damage to the tissue at the anastomotic site.

In this study, voltage is employed to regulate both the temperature at the anastomotic site and the degree of tissue denaturation, while in some literature, power is utilized to achieve this function [23]. When the temperature ranges between 60 and 90 °C, it ensures a certain degree of collagen denaturation, whereas below 60 °C, the extent of collagen denaturation is lower [17, 29]. At a voltage of 40 V, the highest temperature reaches around 60.78 ± 1.9 °C, with a tissue fusion success rate of 20%. Increasing the voltage to 50 V results in a maximum temperature of 79.78 ± 2.451 °C and a tissue fusion success rate of 70%. Furthermore, at 60 V, the highest temperature recorded is 89.25 ± 4.375 °C, achieving a tissue fusion success rate of 100%. This implies that the voltage level determines the maximum temperature at the anastomotic site, and the temperature level influences the degree of collagen denaturation, thereby impacting the quality of the anastomosis. However, it is important to note that higher temperatures also result in increased thermal damage to surrounding tissues [34]. Higher voltage might lead to enhanced anastomotic quality, yet it could also trigger more severe thermal damage, necessitating a delicate balance between the two factors, considering the experimental safety, higher voltages were not attempted in this study.

Maintaining constant initial pressure and voltage while varying the time, we observed a significant improvement in anastomotic quality with prolonged time, which is consistent with conclusions drawn in other literature [4]. When the duration is 10 s, the success rate of the anastomosis is 80%. At 15 s and 20 s, the success rate reaches 100%. However, with an extension from 15 to 20 s, there is a 71% increase in tissue thermal damage. Excessive thermal damage is detrimental to postoperative healing. However, at 15 s and 20 s, there was no statistically significant difference in the highest tissue temperature. This is because the evaporating water vapor carried away heat. Prolonged time can lead to reduced tissue moisture at the anastomotic site, causing significant tissue contraction, and prolonged heat transfer may result in damage to surrounding tissues [23]. In this

study, under the conditions of 250 kPa, 60 V, and 15 s, an effective balance between anastomotic quality and thermal damage was achieved, while variations in optimal fusion parameters across different literature sources [35] are attributed to differences in pulse generator power, electrode size, and tissue characteristics.

Compared to serosa–serosa anastomotic devices [36], the anastomotic device used in this study flips the mucosa outward without the need for additional openings on the intestinal side. This approach avoids secondary damage to the intestine, reduces surgical risks, and prevents intestinal stenosis. During the observation period, the postoperative survival rate of the experimental pigs remained at 100%, with both diet and bowel movements returning to normal within one week. This suggests that utilizing HFEW for intestinal anastomosis demonstrates a certain degree of safety. One month postoperatively, the anastomotic site exhibited excellent recovery with the formation of a durable connection. The surface was smooth with no foreign body overgrowth. The prominent necrotic tissue disappeared, replaced by new tissue. Granulation tissue with new villi formed at the anastomotic site, along with the reshaping of transverse and longitudinal muscles, indicating a progressive improvement in the pathological structure and function of the anastomotic site and signifying the effectiveness of HFEW. However, the collagen fibers in the tissue at the anastomotic site were more abundant compared to normal tissue. Perhaps, more time is needed for the collagen fiber content at the anastomotic site to become entirely identical to that of normal tissue.

This study primarily optimized three crucial experimental parameters, aiming to achieve a consistently stable fusion quality through their combined effects. Further validation of the parameters' effectiveness was conducted using an animal model, laying the foundation for future clinical experiments. However, this study provided a macroscopic assessment of HFEW technology and did not investigate the postoperative tissue status from a molecular biology or immunology perspective, which is a direction for future research. Additionally, extending the observation time span and incorporating more observation time points in the animal model would provide a more comprehensive understanding of the entire recovery process.

The limitation of this study is that the number of in vivo experiments is small; the equipment is in an early stage; and there is no comparison between this technique and existing anastomoses. This is a direction for future research, firstly, to enhance the optimization of the instrumentation to improve the safety and reliability of the procedure; secondly, to optimize the mechanical structure of the anastomosis and to reduce the size of the anastomosis to meet the requirements of the in vivo experiments; and thirdly, to increase the number of experimental animals and to study the healing mechanism of the anastomotic tissues.

Conclusion

In vitro experiments indicate that, with an initial compression pressure of 250 kPa, voltage of 60 V, and time of 15 s, optimal fusion quality can be achieved, with thermal damage controlled within a specific range. The use of a custom-made in vivo intestinal anastomotic device for end-to-end anastomosis resulted in a 100% postoperative survival rate in the animal model, and the tissue at the anastomotic site transitioned from immediate adhesion to permanent adhesion. Both in vitro and in vivo experiments demonstrate the safety and efficacy of end-to-end intestinal anastomosis based on HFEW.

Supplementary Information The online version contains supplementary material available at https://doi.org/10.1007/s00464-024-10795-x.

Acknowledgements We thank many colleagues for their efforts in the early stages of this study, notably Yifan Wang, Li Yin and Wang Hao.

Author contributions CHZ, YYN, XJC, PYX, XDG and LC performed research, CHZ, HZ, JQ, KFL designed research, CHZ and XNT wrote the paper, JBX and KFL acquired funding.

Funding This research was supported by the National Natural Science Foundation of China (51877046) and Pioneering Project of the Academy for Engineering and Technology of Fudan University (gyy2018-002).

Declarations

Disclosures Caihui Zhu, Yuyan Na, Xiujun Cheng, Xiaonan Tao, Pengyao Xie, Lei Chen, Hui Zhao, Jian Qiu, Xiaodong Gu, Jianbin Xiang, and Kefu Liu have no conflicts of interest or financial ties to disclose.

References

1. Neutzling CB, Lustosa SA, Proenca IM, da Silva EM, Matos D (2012) Stapled versus handsewn methods for colorectal anastomosis surgery. Cochrane Database Syst Rev. https://doi.org/10.1002/14651858.CD003144.pub2
2. Santini M, Fiorelli A, Messina G, Laperuta P, Mazzella A, Accardo M (2013) Use of the LigaSure device and the Stapler for closure of the small bowel: a comparative ex vivo study. Surg Today 43:787–793
3. Pan H, Leung KKC, Ng EKW (2020) Tissue fusion technology versus suture and staple in porcine bowel anastomosis: an in vivo study. Braz J Med Biol Res 53:e9305
4. Reyes DA, Brown SI, Cochrane L, Motta LS, Cuschieri A (2012) Thermal fusion: effects and interactions of temperature, compression, and duration variables. Surg Endosc 26:3626–3633
5. Holmer C, Winter H, Kroger M, Nagel A, Jaenicke A, Lauster R, Kraft M, Buhr HJ, Ritz JP (2011) Bipolar radiofrequency induced thermofusion of intestinal anastomoses -feasibility of a

new anastomosis technique in porcine and rat colon. Langenbecks Arch Surg 396:529–533
6. Paton BE, Krivtsun IV, Marinsky GS, Khudetsky IY, Lankin YN, Chernets AV (2013) Welding, cutting and heat treatment of live tissues. Paton Weld J 10:142–153
7. Han S, Cai Z, Ning X, He L, Chen J, Huang Z, Zhou H, Huang D, Zhang P, Li Z (2015) Comparison of a new high-frequency electric welding system for intestinal closure with hand-sewn in vivo pig model. J Laparoendosc Adv Surg Tech A 25:662–667
8. Soreefan AH, Beebeejaun (2013) Electrosurgical bipolar vessel sealing versus conventional clamping and suturing for vaginal hysterectomy: a randomised controlled trial. BJOG Int J Obstet Gynaecol 120:776–777
9. Miyagi K, Rossi SH, Malata CM, Forouhi P (2015) Novel use of LigaSure Impact™ electrosurgical bipolar vessel sealing system in skin-sparing mastectomy. J Plast Reconstr Aesthet Surg 68:e126–e128
10. Metzelder M, Kübler J, Petersen C, Glüer S, Nustede R, Ure B (2006) Laparoscopic nephroureterectomy in children: a prospective study on ligasure™ versus Clip/Ligation. Eur J Pediatr Surg 16:241–244
11. Romano F, Gelmini R, Caprotti R, Andreotti A, Guaglio M, Franzoni C, Uggeri F, Saviano M (2007) Laparoscopic splenectomy: ligasure versus EndoGIA: a comparative study. J Laparoendosc Adv Surg Tech 17:763–768
12. Newcomb WL, Hope WW, Schmelzer TM, Heath JJ, Norton HJ, Lincourt AE, Heniford BT, Iannitti DA (2009) Comparison of blood vessel sealing among new electrosurgical and ultrasonic devices. Surg Endosc 23:90–96
13. Floume TS, Richard RA, Darzi AW, Hanna GB (2010) Optical, thermal, and electrical monitoring of radio-frequency tissue modification. J Biomed Opt 15(1):018003–018003
14. Salameh JR, Schwartz JH, Hildebrandt DA (2006) Can LigaSure seal and divide the small bowel? Am J Surg 191:791–793
15. Kramer EA, Rentschler ME (2018) Energy-based tissue fusion for sutureless closure: applications, mechanisms, and potential for functional recovery. Annu Rev Biomed Eng 20:1–20
16. Sindram D, Martin K, Meadows JP, Prabhu AS, Heath JJ, McKillop IH, Iannitti DA (2011) Collagen–elastin ratio predicts burst pressure of arterial seals created using a bipolar vessel sealing device in a porcine model. Surg Endosc 25:2604–2612
17. Su L, Cloyd KL, Arya S, Hedegaard MA, Steele JA, Elson DS, Stevens MM, Hanna GB (2014) Raman spectroscopic evidence of tissue restructuring in heat-induced tissue fusion. J Biophotonics 7:713–723
18. Zhu C, Yin L, Xu J, Liu H, Xiang X, Zhao H, Qiu J, Liu K (2023) An ex vivo preliminary investigation into the impact of parameters on tissue welding strength in small intestine mucosa-mucosa end-to-end anastomosis. Front Bioeng Biotechnol. https://doi.org/10.3389/fbioe.2023.1200239
19. Hoebeke PB, Zubair S, Oosterlinck W, Verbeeck RMH (1992) Low voltage coagulation for welding sutures watertight an experimental study. Urol Res 20:425–427
20. Wallwiener CW, Rajab TK, Zubke W, Isaacson KB, Enderle M, Schäller D, Wallwiener M (2008) Thermal conduction, compression, and electrical current–an evaluation of major parameters of electrosurgical vessel sealing in a porcine in vitro model. J Minim Invasive Gynecol 15:605–610
21. Winter H, Holmer C, Buhr HJ, Lindner G, Lauster R, Kraft M, Ritz JP (2010) Pilot study of bipolar radiofrequency-induced anastomotic thermofusion-exploration of therapy parameters ex vivo. Int J Colorectal Dis 25:129–133
22. Zhao L, Song C, Wang Z, Zhou Y, Li X, Zhu W, Cuschieri A (2015) Novel concave-convex electrode for colonic anastomoses by radiofrequency thermo-fusion. Surg Endosc 29:1809–1816
23. Zhao L, Zhuo C, Song C, Li X, Zhou Y, Shi D (2015) Histological characteristics of collagen denaturation and injuries in bipolar radiofrequency-induced colonic anastomoses. Pathol Res Pract 211:214–218
24. Yin L, Zhu C, Xu J, Zhao H, Qiu J, Wang H, Liu K (2022) Dynamic impedance analysis of intestinal anastomosis during high-frequency electric field welding process. Sensors (Basel) 22:4101
25. Arya S, Hadjievangelou N, Lei S, Kudo H, Goldin RD, Darzi AW, Elson DS, Hanna GB (2013) Radiofrequency-induced small bowel thermofusion: an ex vivo study of intestinal seal adequacy using mechanical and imaging modalities. Surg Endosc 27:3485–3496
26. Lim CB, Goldin RD, Elson DS, Darzi A, Hanna GB (2010) In vivo thermography during small bowel fusion using radiofrequency energy. Surg Endosc 24:2465–2474
27. Zhu C, Yin L, Xu J, Yang X, Wang H, Xiang X, Liu H, Liu K (2022) Characteristics of collagen changes in small intestine anastomoses induced by high-frequency electric field welding. Biomolecules 12:1683
28. Carr-Locke DL, Day J (2022) Principles of electrosurgery. In: Cohen J (ed) Successful training in gastrointestinal endoscopy. Wilay, Hoboken, pp 143–152
29. Foschi D, Cellerino P, Corsi F, Taidelli T, Morandi E, Rizzi A, Trabucchi E (2002) The mechanisms of blood vessel closure in humans by the application of ultrasonic energy. Surg Endosc 16:814–819
30. van de Berg NJ, van den Dobbelsteen JJ, Jansen FW, Grimbergen CA, Dankelman J (2013) Energetic soft-tissue treatment technologies: an overview of procedural fundamentals and safety factors. Surg Endosc 27:3085–3099
31. Williams JM, Duckworth CA, Burkitt MD, Watson AJM, Campbell BJ, Pritchard DM (2014) Epithelial cell shedding and barrier function: a matter of life and death at the small intestinal villus tip. Vet Pathol 52:445–455
32. Zhao L, Zhou Y, Song C, Wang Z, Cuschieri A (2017) Predicting burst pressure of radiofrequency-induced colorectal anastomosis by bio-impedance measurement. Physiol Meas 38:489–500
33. Gonzalez-Correa CA, Brown BH, Smallwood RH, Walker DC, Bardhan KD (2005) Electrical bioimpedance readings increase with higher pressure applied to the measuring probe. Physiol Meas 26:S39-47
34. Tu L, Zhou Y, Song C, Li Y, Chen L, Xue Y (2019) Preliminary study of a control algorithm for radio-frequency-induced intestinal tissue fusion. Int J Hyperthermia 36:1297–1306
35. Wang Y, Liu K, Xiang X, Zhu C, Wang H (2020) The impedance analysis of small intestine fusion by pulse source. Open Life Sci 15:808–818
36. Kim JS, Park SH, Kim NS, Lee IY, Jung HS, Ahn HM, Son GM, Baek KR (2022) Compression automation of circular stapler for preventing compression injury on gastrointestinal anastomosis. Int J Med Robot Comput Assist Surg. https://doi.org/10.1002/rcs.2374